Electrochemical and spectroscopic evidences of corrosion inhibition of bronze by a triazole derivative

Ahmed Dermaj, Najat Hajjaji, Suzanne Joiret, Kamal Rahmouni, Abdellah Srhiri, Hisasi Takenouti, Vincent Vivier

Electrochemical and spectroscopic evidences of corrosion inhibition of bronze by a triazole derivative

A. Dermaj [a,b], N. Hajjaji [b], S. Joiret [a], K. Rahmouni [a,b],
A. Srhiri [b], H. Takenouti [a], V. Vivier [a,*]

[a] *Laboratoire Interfaces et Systèmes Electrochimiques, UPR 15 du CNRS, Paris, France*
[b] *Laboratoire Electrochimie, Corrosion et Environnement, Faculté des Sciences, Kenitra, Morocco*

The electrochemical behavior of the bronze (Cu–8Sn in wt%) was investigated in 3% NaCl aqueous solution, in presence and in absence of a corrosion inhibitor, the 3-phenyl-1,2,4-triazole-5-thione (PTS). The inhibiting effect of the PTS was evidenced for concentrations higher than 1 mM for the cathodic process whereas its effect was clearly seen with a concentration as low as 0.1 mM for the anodic process. A significant positive shift of the corrosion potential was also observed, and its inhibiting effect increased with both its concentration and the immersion time of the sample. From voltammetry and electrochemical impedance spectroscopy experiments, the inhibiting efficiency of the PTS was found to be in the 94–99% range for 1 mM concentration. Scanning electron microscopy and X-ray energy dispersion analysis of the specimen surface show the presence of sulphur on the surface. Raman micro-spectrometry study confirms the protective effect of the PTS in aqueous solution through three types of interactions with the electrode, namely the adsorption of the inhibitor in a flat configuration, the formation of copper-thiol molecules, and when copper is released, the formation of a polymeric complex.

1. Introduction

Bronze, like brass, is a common structural material, and was one of the first alloys developed by ancient metalworkers. Bronze is a copper alloy containing tin, generally in the 1 to 10% range. The addition of tin increases the bronze hardness making it more resistant to wear when compared with pure copper metal. Nowadays, a large variety of bronze compositions is known, and they may contain various other elements, such as lead, zinc, manganese, aluminium, silicon or iron. The variations of bronze composition (both in proportion and in elemental composition) significantly affect its characteristics, such as providing a higher resistance to wear or improving its machining. For instance, the adjunction of small amount of lead in the bronze composition acts as a lubricant. Such bronzes are often used to make machine parts, like bearings, that must ensure a lot of sliding action against other parts.

However, like all other alloys, bronzes are subjected to corrosion, which results in the formation of an oxide or salt layer on its surface. The oxidized layers can result of either an intentional surface treatment, or a spontaneous origin due to the degradation of the object in various corrosive mediums, for instance due to a burying in the soil during many centuries. In this last case, corrosion products formed on bronze surface, once a sufficient thickness is reached, acquire the barrier property preventing a complete destruction of the object. In this way, the archaeological bronze objects are transmitted up to the present time, even in an aggressive media, such as seawater. The layer of corrosion products is generally named "patina", and when protection of the substrate material is efficient, it is frequently called "beautiful or noble patina" [1–3].

Nevertheless, after the excavation, the sudden change of the environment breaks off the equilibrium obtained over a long period, and sometimes induces an acceleration of the corrosion processes. As a disturbing media, one may mention the

marine and/or urban atmosphere with a high level of pollution. This may lead to a complete decomposition of the archaeological object within a very short period. Consequently, it appears that the use of the protection methods for bronze substrate or the reinforcement of protective property of patina layer become necessary.

The electrochemical study of copper and various Cu–Sn alloys in aqueous solutions are reported by many workers [4–6]. The corrosion inhibitors are easy to apply, reasonable in cost and often efficient to protect these materials. Moreover, the reversibility of the treatments is often required in the conservation of art object. The use of inhibitors is already currently applied as a protective treatment on ancient bronzes. Benzotriazole and its derivatives were shown to be efficient corrosion inhibitors for copper and copper base alloys through the formation of insoluble Cu–BTA complexes on the surface [7–13].

The main objective of this study was to understand the way a triazole inhibitor interacts with a bronze to protect it. Thus, the first part of this work is devoted to study of the corrosion inhibition of a bronze Cu–8%Sn (in wt%) by a triazole derivative, 3-phenyl-1,2,4-triazole-5-thione (PTS) in a NaCl 3% solution. The composition of this alloy is in fact well representative of those of outdoor bronze monuments obtained by casting process. The electrochemical behavior of this bronze was studied by voltammetry and electrochemical impedance spectroscopy (EIS). Its surface state was then characterized by scanning electron microscopy (SEM) coupled with X-ray energy dispersion spectroscopy (EDS) for elemental analysis, and by Raman micro-spectroscopy.

2. Experimental methods

The bronze used in this study, the electrochemical cell and the conditions at which the experiments were performed are briefly presented below.

2.1. Materials and electrode preparation

The alloy used was an industrial bronze, the composition of which was determined by EDS analysis (Fig. 1). This alloy was an as-cast leaded bronze exhibiting a dendritic structure, which was characterized by a low tin (8 wt%) content. However, Fig. 1 clearly evidences that the studied alloy was corresponding to a diphase (Fig. 1b and c) also containing non-miscible lead mostly located in interdendritic spaces (Fig. 1d). The elemental composition of these two phases is reported in Table 1. The amount of tin roughly varies from 5 wt% in the phase I to reach 21 wt% in the phase II. It should also be mentioned that the

amount of white globules in Fig. 1d is corresponding to a very low Pb content bronze. From these analyses, the cartography of phase repartition could be drawn (Fig. 1e). However, some impurities (Zn and Ni) were also detected by EDX analysis, but their amount remains low (Table 1).

For the electrochemical studies, the sample was manufactured to form a right cylinder, the cross-section of which was a disk of 1 cm in diameter (surface area $S = 0.78\,\mathrm{cm}^2$). The lateral part of the bronze rod was firstly protected by a cataphoretic paint (PPG, W781-I292 + W975-G292), heat treated at $150\,^{\circ}\mathrm{C}$ for 30 min, and then molded into an epoxy resin (Buhler, Epoxycure$^{\mathrm{TM}}$). The overall diameter of the electrode, bronze and epoxy resin was 18 mm in diameter. The bronze cylinder was assembled along its axis of rotation allowing its use as a common rotating disk electrode (RDE). Before each experiment, the electrode was abraded with emery papers (from grade 600 to grade 1200), thoroughly rinsed with distilled water, and dried with argon or nitrogen flow. All electrochemical experiments were performed between twice and five times. No significant discrepancy of the results was observed.

The corrosion inhibitor used in this work was a triazole derivative, the 3-phenyl-1,2,4-triazole-5-thione (PTS), synthesized, purified and characterized according to a protocol describes elsewhere [14]. Briefly, this compound was prepared in two steps; a condensation of the thiosemicarbazide with the benzoyl chloride in pyridinic medium to form the 1-benzoylthiosemicarbazide as an intermediate. This reaction was followed by an intra-molecular cyclization in methanol in presence of the sodium methalate. The resulting product was the PTS.

2.2. Electrochemical device

The electrochemical cell was a conventional three-electrode-cell. The reference electrode and the counter electrode were a saturated calomel electrode (SCE) and a large surface platinum grid, respectively. Both the electrochemical cell and the electrometer were placed in a Faraday cage, and all experiments were performed at room temperature. All electrochemical measurements were carried out with a Gamry potentiostat (model PC4/300). The EIS experiments were performed using a $10\,\mathrm{mV_{rms}}$ ac-signal at the open circuit corrosion potential (E_{oc}) from 50 kHz to 10 mHz with 10 points per decade. The results presented in this study were obtained in 3% NaCl solution prepared from doubly distilled water.

2.3. Techniques

Scanning electron microscopy (SEM) studies were performed with a Leica Stereoscan 440 coupled with EDS elemental semi-quantitative analyses (Princeton Gamma-Tech) at 20 keV and 5.3 nA.

The Raman spectroscopy was carried out with a Labram–Jobin–Yvon spectrometer. The samples were irradiated with a helium neon laser at $\lambda = 632.8\,\mathrm{nm}$. The laser power was varied between 0.1 and 1 mW to avoid any thermal effect on sample during the analyses. A confocal microscope was used

Table 1

Composition of the bronze determined by EDX analysis (only element with a significant percentage were reported)

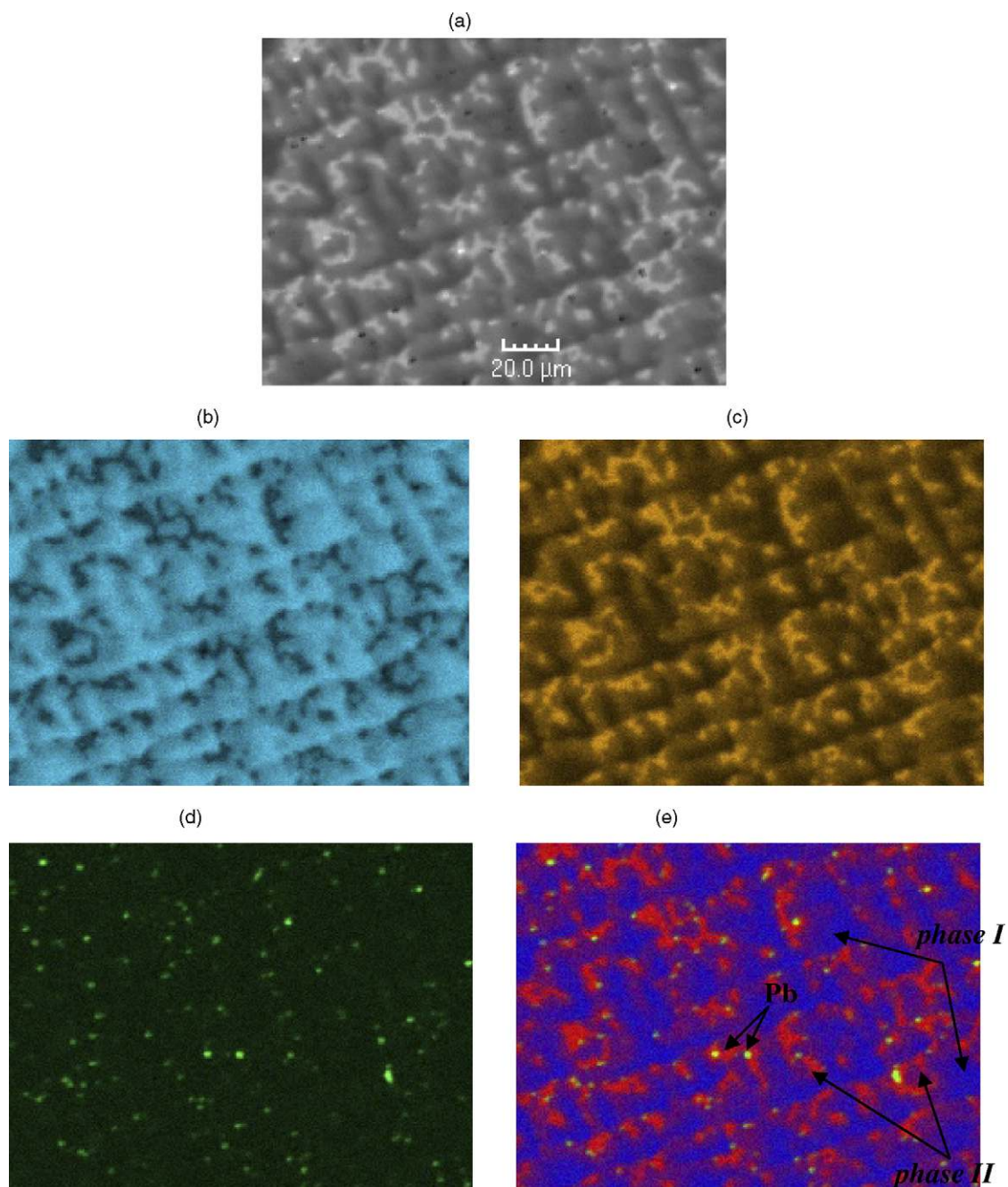|	Sn	Pb	Ni	Zn	Cu
Phase I (wt%)	5.12	0.59	0.39	0.79	93.11
Phase II (wt%)	21.29	1.69	0.38	0.29	76.35

Fig. 1. SEM image of the bronze (a), quantitative EDX analyses element by element Cu (b), Sn (c) and Pb (d). Image (e) shows the different phases of the bronze and was obtained from EDX results (phase analysis).

and the investigated area was limited to $1.2\,\mu m^2$ using an 80 ULWD objective lens.

3. Results and discussion

3.1. Voltammetry experiments

The cathodic and anodic polarization curves of the bronze obtained with a RDE at 1000 rpm in 3% NaCl solution with various PTS concentrations are presented in Figs. 2 and 3, respectively. The range of PTS concentrations investigated in

this work was limited since the solubility of the synthesized compound was quite low (between 1 and 1.2 mM). All of these curves were obtained after 1 h immersion of the electrode in the electrolytic solution at open circuit potential (E_{oc}). Then cathodic and anodic polarization curves were recorded from independent experiments. The initial potential was stated at a slightly more positive potential from E_{oc} for the cathodic scans, and conversely, it was set at a slightly more negative value from E_{oc} for the anodic scans.

In absence of PTS, the cathodic current (Fig. 2) follows the Tafel law for $E > -0.5$ V/SCE, and then the corrosion the corrosion current density can be determined readily ($I_{corr} \approx$
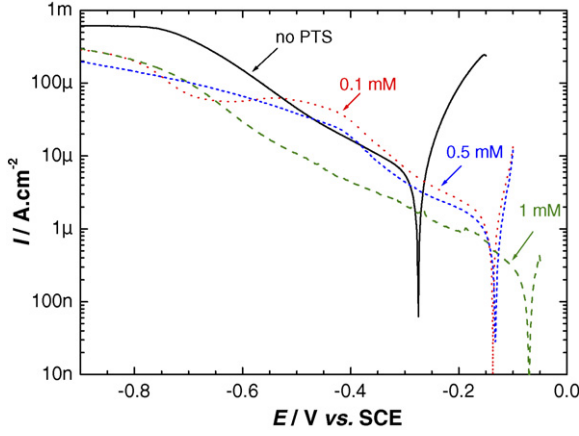
Fig. 2. Cathodic polarization curves of the bronze in a 3% NaCl solution with various PTS concentrations (1000 rpm, $\nu = 1\,\mathrm{mV\,s^{-1}}$).
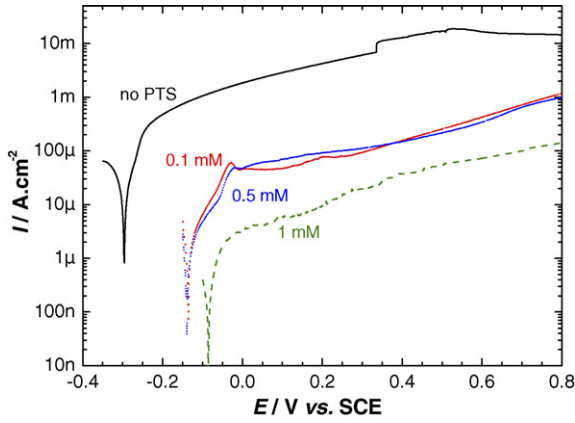

Fig. 3. Anodic polarization curves of the bronze in a 3% NaCl solution with various PTS concentrations (1000 rpm, $\nu = 1\,\mathrm{mV\,s^{-1}}$).

$7\,\mu\mathrm{A\,cm^{-2}}$). For potential more negative than -0.7 V/SCE, the current plateau observed is ascribed to the limiting current of the dissolved oxygen reduction [15]. The adding of 0.1 or 0.5 mM of PTS into the corrosive medium is accompanied by both a shift of E_{corr} toward more positive potential, and by a decrease of I_{corr}. It is important to point out that for potential more positive than -0.5 V/SCE, the Tafel slope is independent of the inhibitor concentration. In contrast, the cathodic curves in the most negative potential domain (Fig. 2) are different in presence and in absence of PTS, namely, the limiting current corresponding to the oxygen reduction is always observed but its value is three to five times lower than in absence of PTS. This may be explained, for instance, by the formation of surface film which hinders the diffusion of dissolved oxygen towards

the electrode surface in addition to the hydrodynamic diffusion layer.

Close to the open circuit corrosion potential, that is where a linear behavior is expected, the Stern–Geary relationship [16] was considered to be valid:

$$I = I_{corr}\{\exp[b_a(E - E_{corr})] - \exp[b_c(E - E_{corr})]\} \qquad (1)$$

where b_a and b_c are the anodic and cathodic activation coefficients, respectively. A non-linear regression calculation was applied to evaluate these kinetic parameters, and the results of calculation are reported in Table 2. In all cases, the correlation factor R^2 was greater than 99% indicating a good fitting result. The confident interval for I_{corr} is in the order of one percent whereas E_{corr} was determined with an error margin lower than 1 mV. As stated above, the cathodic Tafel constant b_c remains essentially constant with PTS concentration whereas the anodic Tafel constant b_a becomes very huge in presence of the inhibitor. This phenomenon can be explained by desorption of the inhibitor when the potential shifted towards more anodic direction as previously reported by Epelboin et al. [17].

The inhibitor efficiency (IE) in percent was evaluated from the following relationship:

$$\mathrm{IE}\,(\%) = 100 \times \frac{I_{corr}^0 - I_{corr}}{I_{corr}^0} \qquad (2)$$

where I_{corr}^0 and I_{corr} denote the corrosion currents densities in absence and in presence of inhibitor, respectively. The inhibiting efficiency increases with the PTS concentration for a given temperature and immersion time, and it reaches 96% for the addition of 1 mM PTS.

In absence of inhibitor, the anodic curve (Fig. 3) exhibits two distinct domains: the first zone is located in the vicinity of the corrosion potential and is characterized by a steep Tafel slope whereas the second zone located towards more positive potentials is characterized by a quite constant current density. This limiting current density is likely governed by the solubility of CuCl salt layer [18].

The addition of corrosion inhibitor into the solution is accompanied by a significant decrease of the anodic current density which is more marked near E_{corr}. For instance, at 0 V/SCE, the anodic current density is divided by a factor 20 for a 0.5 mM PTS and by a factor 300 when the PTS concentration reaches 1 mM. These results are fully compatible with the presence of a compact surface film composed of the corrosion products formed during the initial stage of the experiment, that is, when the sample is left at its rest potential for 1 h.

E_{corr} and the kinetic parameters determined by a non-linear regression calculation from the anodic polarization scans close

Table 2
Values determined from the non-linear regression calculation for the Stern–Geary relationship for the experimental results presented in Fig. 2

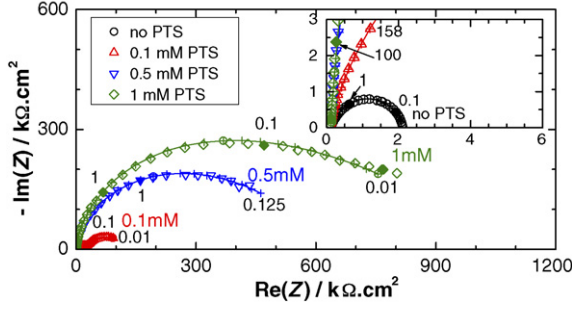| [PTS] (mM)	E_{corr} (V vs. SCE)	I_{corr} ($\mu\mathrm{A\,cm^{-2}}$)	b_c ($\mathrm{V^{-1}}$)	b_a ($\mathrm{V^{-1}}$)	IE (%)
0	-0.298	7.35	-9.28	24.9	–
0.1	-0.135	1.37	-9.18	62.7	81.6
0.5	-0.130	0.938	-8.88	79.9	87.2
1	-0.077	0.302	-10.6	33.4	95.9

Fig. 4. EIS spectra of bronze in a 3% NaCl solution for various PTS concentrations obtained after 1 h immersion at rest potential (1000 rpm). The crosses (+) on each diagram correspond to the simulated spectrum.
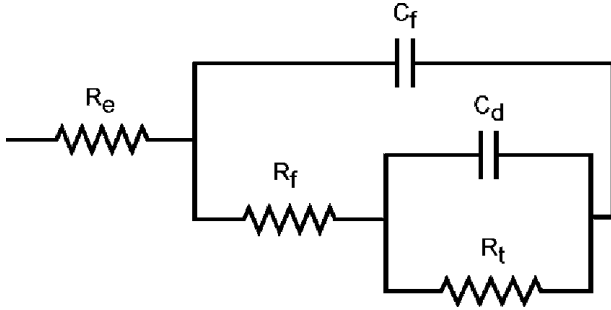

Fig. 5. Electrical equivalent circuit used to simulate EIS data for the bronze corrosion in 3% NaCl solution without inhibitor.

to the open circuit potential are similar to those determined for the cathodic scans, though I_{corr} is slightly higher. The inhibiting efficiency at different PTS concentrations is also similar to those presented in Table 2.

3.2. Electrochemical impedance spectroscopy (EIS)

We will firstly determine the effect of the inhibitor concentration for a given immersion time, here 1 h, and then the influence of immersion period will be estimated.

3.2.1. Influence of PTS concentration

Fig. 4 shows EIS spectra collected after 1 h of immersion of the bronze in the electrolytic solution at the rest potential with and without PTS.

In absence of inhibitor, the Nyquist diagram presents a flattened semi-circle with a deformation in the high frequency domain as shown on the insert of Fig. 4. Assuming that this impedance data can be described by two R and C ladder circuits (Fig. 5), the impedance spectrum could be fitted suitably. As a matter of fact, the cross symbol on Fig. 4, obtained by a

non-linear regression calculation is close to experimental data. The addition of the PTS at various concentrations also displays a capacitive behavior of the alloy in the NaCl medium (Fig. 4). The polarization resistance R_p determined from the extrapolation of the impedance spectra towards the low frequency limit, increases with the inhibitor concentration. R_p is about $2\,\mathrm{k\Omega\,cm^2}$ in 3% NaCl solution without PTS, whereas it reaches 100, 600 and $900\,\mathrm{k\Omega\,cm^2}$ for PTS concentrations of 0.1, 0.5 and 1 mM, respectively. However, these diagrams cannot be explained with only two R and C circuits displayed in Fig. 5, and thus, a third R–C circuit was added. The use of such an electrical equivalent circuit is in agreement with the previous results presented and discussed in the references [19,20]. Those R–C couples are ascribed to the following contributions: The high frequency contribution (C_f–R_f) is ascribed to the dielectric character of the corrosion products (C_f) due to the formation of thin surface film that is reinforced by the presence of the inhibitor and by the ionic conduction through the pores of the film (R_f). The medium frequency contribution is attributed to the double layer capacitance (C_d) at the electrolyte/bronze interface at the bottom of the pores coupled with the charge transfer resistance (R_t), whereas the low frequency elements are related to the oxidation–reduction contribution of the corrosion products (R_F–C_F). There is no contribution of the latter couple in the absence of inhibitor. Moreover, the values determined for this couple from the numerical simulations of the ac diagrams are not discussed in the text since it appears that they are scattered probably due to the fact that they are likely ascribed to corrosion products.

The values determined from a non-linear regression calculation for C_f–R_f and R_t–C_d couples are summarized in Table 3. In this calculation, in stead of a pure capacitance, the distribution of the time constant for R–C couple was used.

$$Z = \frac{R}{1 + (j \times \omega \times \tau)^n}, \quad \text{where } \tau = R \times C \qquad (3)$$

Here, n is a fractional number comprised between 0 and 1. The use of this parameter, similar to the constant phase element (CPE), allowed the depressed feature of Nyquist plot to be reproduced readily. However, in contrast to CPE, the distribution of time constant τ would be involved in the capacitance as well as in the resistance.

It is shown that the capacitance C_f decreases with the PTS concentration. In absence of inhibitor, C_f is about $10\,\mu\mathrm{F\,cm^{-2}}$, which corresponds to a contribution of a very thin layer. Assuming that the permittivity ε of the patina is similar to that of the cuprite Cu_2O, that is, $\varepsilon = 12$ [21], the thickness of film, d, can

Table 3
Parameters determined by non-linear regression of the results presented in Fig. 3

[PTS] (mM)	C_f (μF cm^{-2})	R_f (kΩ cm^2)	C_d (μF cm^{-2})	R_t (kΩ cm^2)	IE (%)
0	8.23	0.331	67.5	1.69	–
0.1	0.488	22.2	11.2	138	98.8
0.5	0.428	115	7.25	255	99.3
1	0.347	342	2.17	695	99.8

be evaluated by the following relationship:

$$C_{\mathrm{f}} = \frac{\varepsilon \times \varepsilon_0 \times A}{d} \qquad (4)$$

where A is the electrode surface area and ε_0 is the permittivity of the vacuum. In this calculation, the surface roughness was neglected, and a thickness of 1.2 nm was determined. Such a value corresponds to about three monolayers of cuprite. In presence of 1 mM PTS, C_{f} decreased by a factor of 24, compared with the solution without inhibitor. In the same time, R_{f} increased by 1000. That is, the ionic conductivity of surface film significantly decreases in the presence of the inhibitor, much more than that expected for the mere change of the film thickness. Assuming that the ionic conduction through film is ensured by pores crossing the both sides of film, and taking account of the increase of film thickness, the total surface of pores should then be divided by 40. As a result, the capacitance C_{d} corresponds to the contribution of the surface of the bronze in contact with the electrolytic solution at the pore bottom would be divided by the same factor. Table 3 indicates that C_{d} decreased by the factor of 30. Thus, these calculations corroborate the model of porous layer used in this study. The value of n for the surface film is close to 1, which indicates relatively uniform surface film.

The charge transfer resistance increases by a ratio of 400 in the presence of 1 mM PTS. This indicates that the inhibiting effect of PTS is not only due to the decrease of the surface area in contact with electrolyte, but also to the slowing down of the charge transfer process at the interface. The inhibiting effect of the PTS can also be assessed, assuming that I_{corr} is reciprocally proportional to R_{t}:

$$\mathrm{IE}\,(\%) = 100 \times \frac{R_{\mathrm{t}} - R_{\mathrm{t}}^0}{R_{\mathrm{t}}} \qquad (5)$$

IE(%) is then larger than 99% when 1 mM of PTS is added in the 3% NaCl solution. However, one should keep in mind that Eq. (5) gives a way to evaluate the inhibitor efficiency taking the R_{t} value without inhibitor as reference. Thus, even if the difference between IE = 98.8% (obtained for 0.1 mM PTS) and IE = 99.8% (obtained for 1 mM PTS) seems to be small, it corresponds in reality to a significant improvement of the corrosion protection by the PTS.

3.2.2. Influence of the immersion time

Fig. 6 presents the effect of the immersion time on the impedance spectra at the corrosion potential. The inhibitor concentration was set at 1 mM. The shape of these curves is very similar to that obtained when varying the inhibitor concentration. The polarization resistance (determined at the low frequency limit of the impedance spectrum) changes from about 1 $\mathrm{M\Omega\,cm^2}$ after 1 h to approximately 5.5 $\mathrm{M\Omega\,cm^2}$ after 20 h immersion. This increase illustrates the protective effect of the PTS, which is reinforced with the immersion time.

The Fig. 7a shows the surface state of bronze used before the experiment, that is, before the immersion of the electrode in the electrolytic solution. As discussed in the experimental section, its surface is inhomogeneous. The white spots correspond to Pb-rich zones as it was already observed on an archaeological
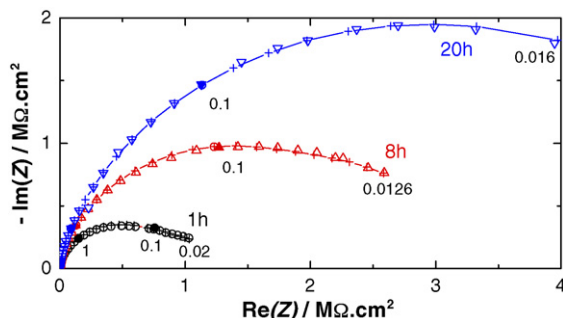

Fig. 6. EIS spectra of bronze in a 3% NaCl solution after various immersion time in 3% NaCl + 1 mM PTS solution at rest potential (1000 rpm). The crosses (+) on each diagram correspond to the simulated spectrum.

bronze coin of the Post Roman Empire discovered in Morocco [22]. After the immersion of the bronze electrode in a 3% NaCl solution (Fig. 7b), corrosion products form a cracked film on the electrode surface. However, in presence of PTS (Fig. 7c), the whole surface of the bronze appears to be poorly affected by corrosion and it should be mentioned that even the lead globules appear to be not dissolved. The surface analysis by EDS (not presented here) shows the presence of oxygen and chloride in addition to the three major elements (Cu, Sn and Pb) when bronze was immersed in NaCl 3% with or without inhibitor. The corrosion products would be thus mainly in the oxide form. Moreover, in the presence of inhibitor, sulphur characterizing the presence of PTS at the film surface was evidenced.

3.3. Raman spectroscopy

The three Raman spectra collected on the bronze electrode when immersed in NaCl solution with 1 $\mathrm{mM\,L^{-1}}$ of PTS, with real intensity in counts $\mathrm{s^{-1}}$ coming from the nearest part of the metal (a) up to the interface of corrosion products with solution (c) are depicted in Fig. 8. These in-depth profiles were obtained thanks to the confocal microscope.

Raman spectrum of PTS in solid state is shown in Fig. 9a, the same spectrum is re-plotted in Fig. 9b in enlarged scale by truncating the three main bands marked by "*" and ascribable to the phenyl group. The spectrum of methyl-triazole thione (MTS) is presented in Fig. 9c.

3.3.1. Reference spectra

Due to the scarceness of reference data for the attribution of the Raman bands to the vibration modes of PTS, Raman spectra of reference products were recorded. As this work is not devoted to an assignment of PTS vibration modes, only the bands useful for the interpretation of the compounds found on bronze electrode were analyzed. For simplicity, various bands reported in the literature for similar compounds are summarized in Table 4: the triazole [23], the triazolethione [24], the 3-mercaptotriazole [25] and the triazolethione anion for the triazole moiety [26].

The two products used as references are clearly in thione form since the band characteristic of thiol function [25] at 2555 $\mathrm{cm^{-1}}$ is not observed in the Raman spectra (not shown for methyl). According to literature data [24–26] the band at
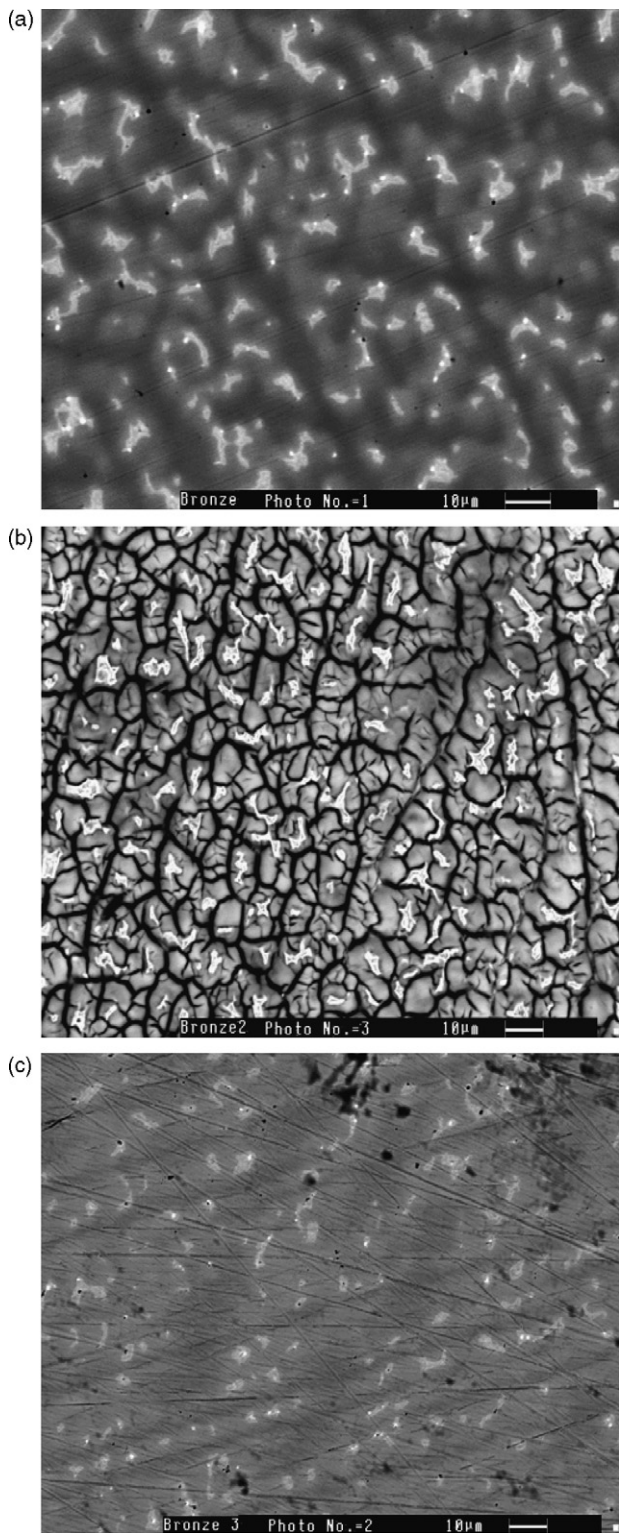
Fig. 7. Back-scattered electron image of the bronze before corrosion experiment (a), and after 10 h immersion (1000 rpm) in 3% NaCl solution (b) and in 3% NaCl solution + 1 mM de PTS (c).

Table 4
Raman vibration modes of various groups for the attribution of PTS vibration modes

| Methyl-triazole thione	Phenyl-triazolethione	Phenyl	Complex	Phenyl ads	Triazolethione [17]	Triazolethione anion [19]	Mercaptotriazole [18]	Triazole [16]
1600	1585		1606		1555 r_1	1503 C=N	1560 C=N	1537 r_1 stretch
			1520			1450 C_s=N	1467 C=N	
1485	1485		1440		1475 r_2		1432 N=C	1486 r_2, stretch
1365	1360				1320 r_3	1304 N=C—N		1380 r_3 stretch
						1274 C_s—N		
1220	1210				1260 r_4	1190 N=C	1254 N—N	1260 r_4 stretch 1148 r_5 breath
1030	1028				1140 r_5	1090 N—N 1008 ring breath		
		1002 ν_{12}		966				
975	970	810, 795 ν_{10}, ν_{11}		791, 766	985, 945 r_6, r_7 i.p. bend	980 r_6, r_7 i.p. bend	999 r_6, r_7 i.p. bend	982, 964 r_6, r_7 i.p. bend
		618 ν_{6b}			670, 625 r. o.p. bend		501 r. o.p. bend	680, 650 r. o.p. bend
1345	1325				1425, 1060 N—H bend		1200 N—H bend	1187 N—H bend
428	425		701		525 C=S	505 C—S⁻	707 C—(SH) bend	
							2555 S—H stretch	
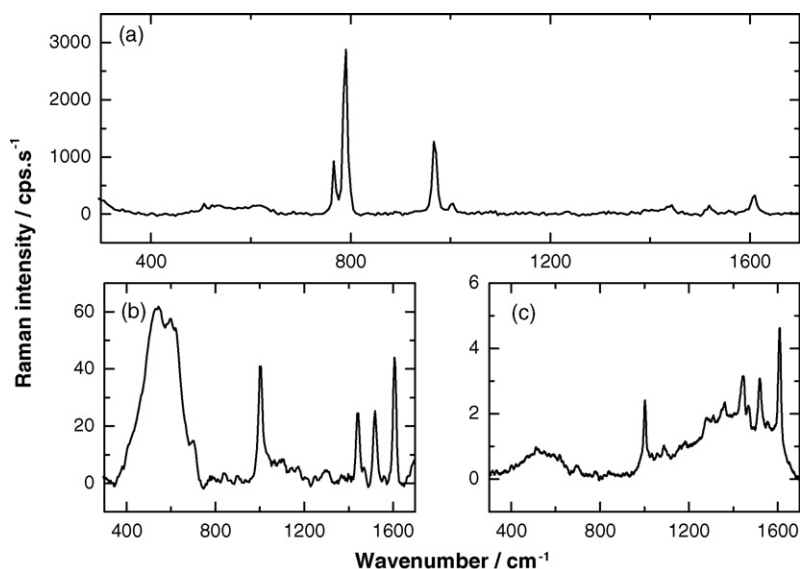
Fig. 8. Raman spectra collected on the bronze electrode after 1 h of immersion in NaCl + 1 mM L^{-1} PTS (1000 rpm), coming from the nearest part of the metal (a and b) up to the interface of corrosion products with solution (c) (real intensity in counts s^{-1}).

422 cm^{-1} (phenyl)–427 cm^{-1} (methyl) is to be attributed to C=S vibration.

The four main bands at 1002, 810, 795 and 618 cm^{-1} on PTS spectrum are due to phenyl vibration as they are absent in methyl spectrum. Moreover, their value are in accordance with those reported for substituted benzene and their modes, respectively, trigonal ring breathing ν_{12}, umbrella ν_{11} and ν_{10} (both C–H out of plane) and in plane ring bending ν_{6b}, are deduced from references [27,28].

In order to compare with the methyl spectrum these bands are reduced in Fig. 9b. The common features of the two spectra have to be attributed to triazole unit: a red shift of triazole bands is observed when changing from phenyl to methyl substitute more pronounced comparing them with non-substituted triazole. The six main ring vibrations are observed and the same frequency shift (100 cm^{-1}) between single (ν_2) and double (ν_1) bonded C–N stretching vibrations is measured as for all the ref-

erences compounds from Table 4. Values for N–H bending are given without any confidence as they are clearly dispersed in the reference data.

3.3.2. Corrosion layer

The two bands at 470 and 620 cm^{-1} are characteristic of the passive "oxide" layer on copper in neutral solution [29,30] showing that the inhibitive property of the molecule is not complete as already determined from electrochemical results. These bands appear in the three spectra.

However, Raman bands characteristic of organic compounds are clearly detected on the three spectra. It is important to recall that the inhibitor solution (at the concentration used in this study) does not give any evidence of Raman signal coming from organics. Therefore, the Raman spectra observed here is indeed related to the species adsorbed on the bronze surface, only.

The huge intensity of spectrum (Fig. 8a) can be attributed to a surface enhanced Raman scattering (SERS) effect coming from the roughness of the copper part of the metal still suffering a corrosion process. The fact that this spectrum is characteristic of the part of the corrosion product nearest to the surface is also in favor of a SERS mechanism as the enhancement of Raman spectra is confined to a layer thickness of a few nanometers. In this case, the vibration modes having dipole changes perpendicular to the surface are expected to show the greatest enhancement [31].

The three main bands observed in the spectrum correspond to phenyl vibration with a red shift due to interaction with the surface through π-electrons from the ring. The bands corresponding to C–H out of plane vibrations are the greatest in this spectrum suggesting that phenyl ring is almost flat on the copper surface leading to the greatest enhancement for vibrations perpendicular (out of plane) to it.

The second spectrum still shows the main band of phenyl part of the inhibitor but fairly less intense. Now, the bands corresponding to the triazole moiety are clearly displayed in
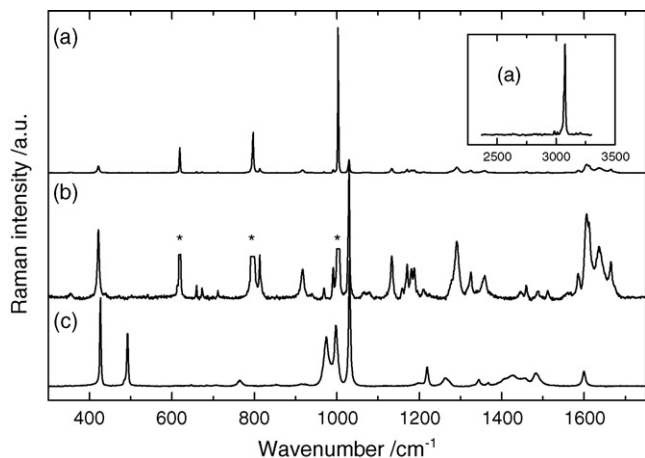

Fig. 9. (a) Raman spectrum of PTS in solid state, (b) same spectrum re-plotted in in enlarged scale by truncating the three main bands marked by "*" and (c) spectrum of methyl-triazole thione (MTS).

this spectrum with two new features: a band at $1520\,\mathrm{cm}^{-1}$ and another one on the side of copper passive layer spectrum at $701\,\mathrm{cm}^{-1}$. This last value is close to the band measured at $707\,\mathrm{cm}^{-1}$ in mercaptotriazole and attributed to C−SH unit. Formation of a thiol complex between copper and PTS (or adsorption of the molecule by sulphur through a thiol bonding) is already indicated by this band. The new band at $1520\,\mathrm{cm}^{-1}$, in the range of C=N vibration values, is also in favor of this mechanism together with the frequency decrease of the band at $1485\,\mathrm{cm}^{-1}$ appearing now at $1440\,\mathrm{cm}^{-1}$ in the spectrum. The band at $1520\,\mathrm{cm}^{-1}$ can be attributed to the new C=N bond formed in the thiol form of the molecule and frequency shift to the weakening of C−NH though those bands are known as not pure vibration modes [32]. The Raman spectrum observed in the intermediate part of the corrosion layer shows that a bond exists between copper and the inhibitor in the thiol form.

The third Raman spectrum (the less intense one), observed at the external part of corrosion products is much more difficult to interpret due to the lack of definition of bands in the range $1200–1600\,\mathrm{cm}^{-1}$. However, it is known [33] that triazole form with copper ions (cuprous and cupric forms) polymeric complexes where two copper ions are bounded with the same triazole molecule (with two different nitrogen in the case of triazole and one sulphur and one nitrogen in the case of triazolethione). Raman spectrum in this case is expected to give a large band extending from 1100 to $1600\,\mathrm{cm}^{-1}$ like in the case of polyaniline [34] but in this polymer, resonance allows the separation of the various contributions.

4. Conclusions

Thanks to the combination of electrochemical impedance and Raman spectroscopies, the behavior of bronze electrode in NaCl solution in presence of 3-phenyl-1,2,4-triazole-5-thione inhibitor has been elucidated. In presence of PTS, it was shown that both anodic and cathodic processes are inhibited. Electrochemical impedance measurements also evidenced the formation of a compact thin-film. The good inhibitive properties of the PTS molecule were ascribed to its adsorption on the metal surface in combination with the release of ions in solution increasing the patina compactness and decreasing the ingress of aggressive anions. Electrochemical measurements gave a quantification of these phenomena through the inhibition efficiency coefficient and the pore dimensions.

Acknowledgements

References

[1] L. Robbiola, J.-M. Blengino, C. Fiaud, Corros. Sci. 40 (1998) 2083.
[2] L. Robbiola, C. Fiaud, Revue d'archéométrie 16 (1992) 109.
[3] M. Aucouturier, M. Keddam, L. Robbiola, H. Takenouti, Techné (2003) 86.
[4] L. Robbiola, N. Pereira, K. Thaury, C. Fiaud, J.-P. Labbé, in: W. Mourey, L. Robibola (Eds.), Decuprification Phenomenon of Cu–Sn Alloys in Aqueous Solution at Nearly Neutral pH Condition in METAL 98, James & James Science Publisher, London, 1998, p. 136.
[5] E. Sidot, N. Souissi, L. Bousselmi, E. Triki, L. Robbiola, Corros. Sci. 48 (2006) 2241.
[6] M. Fabrizi, H. Ganairis, S. Tarling, D.A. Scott, Stud. Conserv. 34 (1983) 45.
[7] G.P. Poling, Corros. Sci. 10 (1970) 359.
[8] Y.C. Wu, P. Zang, H.W. Pickering, D.L. Allara, J. Electrochem. Soc. 140 (1993) 2791.
[9] D. Thierry, C. Leygraf, J. Electrochem. Soc. 132 (1985) 1009.
[10] M.M. Musiani, G. Mengoli, M. Fleischmann, R.B. Lowry, J. Electroanal. Chem. 217 (1987) 187.
[11] C. Törnkvist, D. Thierry, J. Bergman, B. Liedberg, C. Leygraf, J. Electrochem. Soc. 136 (1989) 55.
[12] M. Ito, M. Takahashi, Surf. Sci. 158 (1985) 609.
[13] S. Mamas, T. Kıyak, M. Kabasakaloglu, A. Koc, Mater. Chem. Phys. 93 (2005) 41.
[14] D. Chebabe, A. Dermaj, Z. Ait Chikh, N. Hajjaji, Synth. Commun. 34 (2004) 1.
[15] Z. Ait Chikh, Doctoral Dissertation, Ibn Tofail University, Kenitra, Morocco, 2001.
[16] M. Stern, A.L. Geary, J. Electrochem. Soc. 104 (1957) 56.
[17] I. Epelboin, Ph. Morel, H. Takenouti, J. Electrochem. Soc. 118 (1971) 1282.
[18] E. D'Elia, O.E. Barcia, O.R. Mattos, N. Pébère, B. Tribollet, J. Electrochem. Soc. 143 (1996) 961.
[19] B. Trachli, Co-tutelle Doctoral Dissertation, P&M Curie University (France), Ibn Tofail University, Morocco, 2001.
[20] K. Rahmouni, M. Keddam, A. Srhiri, H. Takenouti, Corros. Sci. 47 (2005) 3249.
[21] B. Tamamushi, S. Toyama, M. Kotani, E. Andoh, H. Takahashi, R. Kubo, S. Nagaura, T. Inoue, Chemical Handbook, Iwanami Editor, Tokyo, 1971 (in Japanese).
[22] M. Serghini-Idrissi, M.C. Bernard, F.Z. Harrif, S. Joiret, K. Rahmouni, A. Srhiri, H. Takenouti, V. Vivier, M. Ziani, Electrochim. Acta 50 (2005) 4699.
[23] D. Bougeard, N. Le Calve, B. Saint Roch, A. Novak, J. Chem. Phys. 64 (1976) 5152.
[24] A. Elhajji, N. Ouijja, M.S. Idrissi, C. Garrigou-Lagrange, Spectrochim. Acta 53A (1997) 699.
[25] V. Krishnakumar, R.J. Xavier, Spectrochim. Acta 60A (2004) 709.
[26] B. Pergolese, A. Bigotto, J. Mol. Struct. 651–653 (2003) 349.
[27] C.S. Korman, R.V. Coleman, Phys. Rev. B 15 (1977) 1877.
[28] E.B. Wilson, J. Phys. Rev. B 45 (1934) 706.
[29] G. Niaura, Electrochim. Acta 45 (2000) 3507.
[30] H.Y. Chan, C.G. Takoudis, M.J. Weaver, J. Phys. Chem. B 103 (1999) 357.
[31] G.C. Schatz, R.P. Van Duyne, Surf. Sci. 101 (1980) 425.
[32] F. Billes, H. Endredi, G. Keresztury, J. Mol. Struct. THEOCHEM 530 (2000) 183.
[33] L. Yi, L.N. Zhu, B. Ding, P. Cheng, D.Z. Liao, Y.P. Zhai, S.P. Yan, Z.H. Jiang, Trans. Met. Chem. 29 (2004) 200.
[34] M.-C. Bernard, V.T. Bich, S. Cordoba de Torresi, A. Hugot-Le Goff, Synth. Met. 84 (1997) 785.